Inorg. Chem. **2003**, *42*, 7519–7530

Role of Carboxylate Bridges in Modulating Nonheme Diiron(II)/O_2 Reactivity

Miquel Costas,[†] Clyde W. Cady,[†] Sergey V. Kryatov,[‡] Manabendra Ray,[†] Meghan J. Ryan,[†] Elena V. Rybak-Akimova,*[,‡] and Lawrence Que, Jr.*[,†]

Department of Chemistry and Center for Metals in Biocatalysis, University of Minnesota, Minneapolis, Minnesota 55455, and Department of Chemistry, Tufts University, Medford, Massachusetts 02155

Received April 2, 2003

A series of diiron(II) complexes of the dinucleating ligand HPTP (*N,N,N′,N′*-tetrakis(2-pyridylmethyl)-2-hydroxy-1,3-diaminopropane) with one or two supporting carboxylate bridges has been synthesized and characterized. The crystal structure of one member of each subset has been obtained to reveal for subset A a (μ-alkoxo)(μ-carboxylato)-diiron(II) center with one five- and one six-coordinate metal ion and for subset B a coordinatively saturated (μ-alkoxo)bis(μ-carboxylato)diiron(II) center. These complexes react with O_2 in second-order processes to form adducts characterized as (μ-1,2-peroxo)diiron(III) complexes. Stopped-flow kinetic studies show that the oxygenation step is sensitive to the availability of an O_2 binding site on the diiron(II) center, as subset B reacts more slowly by an order of magnitude. The lifetimes of the O_2 adducts are also distinct and can be modulated by the addition of oxygen donor ligands. The O_2 adduct of a monocarboxylate complex decays by a fast second-order process that must be monitored by stopped-flow methods, but becomes stabilized in CH_2Cl_2/DMSO (9:1 v/v) and decomposes by a much slower first-order process. The O_2 adduct of a dicarboxylate complex is even more stable in pure CH_2Cl_2 and decays by a first-order process. These differences in adduct stability are reflected in the observation that only the O_2 adducts of monocarboxylate complexes can oxidize substrates, and only those substrates that can bind to the diiron center. Thus, the much greater stability of the O_2 adducts of dicarboxylate complexes can be rationalized by the formation of a (μ-alkoxo)(μ-1,2-peroxo)diiron(III) complex wherein the carboxylate bridges in the diiron(II) complex become terminal ligands in the O_2 adduct, occupy the remaining coordination sites on the diiron center, and prevent binding of potential substrates. Implications for the oxidation mechanisms of nonheme diiron enzymes are discussed.

Introduction

Investigations of dioxygen binding and activation at dinuclear iron complexes have been motivated by the presence of carboxylate bridged dinuclear iron sites in dioxygen activating enzymes such as ribonucleotide reductase (RNR), methane monooxygenase (MMO), and fatty acid desaturases.[1−3] In the first step of oxygen activation, the diiron(II) center is proposed to bind oxygen to form a diiron(III)−peroxo adduct, which then undergoes O−O bond cleavage in a subsequent step. Spectroscopically observable but distinct high valent intermediates have been observed for RNR[4−6] and MMO.[7−10] The observation of such species in the enzyme

* To whom correspondence should be addressed. E-mail: erybakak@tufts.edu (E.V.R.-A.); que@chem.umn.edu (L.Q.).
[†] University of Minnesota.
[‡] Tufts University.

(1) Wallar, B. J.; Lipscomb, J. D. *Chem. Rev.* **1996**, *96*, 2625−2658.
(2) Solomon, E. I.; Brunold, T. C.; Davis, M. I.; Kemsley, J. N.; Lee, S.-K.; Lehnert, N.; Neese, F.; Skulan, A. J.; Yang, Y.-S.; Zhou, J. *Chem. Rev.* **2000**, *100*, 235−349.
(3) Merkx, M.; Kopp, D. A.; Sazinsky, M. H.; Blazyk, J. L.; Müller, J.; Lippard, S. J. *Angew. Chem., Int. Ed.* **2001**, *40*, 2782−2807.
(4) Bollinger, J. M., Jr.; Edmondson, D. E.; Huynh, B. H.; Filley, J.; Norton, J.; Stubbe, J. *Science* **1991**, *253*, 292−298.
(5) Sturgeon, B. E.; Burdi, D.; Chen, S.; Huynh, B.-H.; Edmondson, D. E.; Stubbe, J.; Hoffman, B. M. *J. Am. Chem. Soc.* **1996**, *118*, 7551−7557.
(6) Riggs-Gelasco, P. J.; Shu, L.; Chen, S.; Burdi, D.; Huynh, B. H.; Que, L., Jr.; Stubbe, J. *J. Am. Chem. Soc.* **1998**, *120*, 849−860.
(7) Lee, S.-K.; Nesheim, J. C.; Lipscomb, J. D. *J. Biol. Chem.* **1993**, *268*, 21569−21577.
(8) Lee, S.-K.; Fox, B. G.; Froland, W. A.; Lipscomb, J. D.; Münck, E. *J. Am. Chem. Soc.* **1993**, *115*, 6450−6451.
(9) Liu, K. E.; Valentine, A. M.; Wang, D.; Huynh, B. H.; Edmondson, D. E.; Salifoglou, A.; Lippard, S. J. *J. Am. Chem. Soc.* **1995**, *117*, 10174−10185.

10.1021/ic034359a CCC: $25.00
Published on Web 10/18/2003

reactions has stimulated efforts to generate and characterize analogous intermediates in model systems to serve as synthetic inorganic precedents for the chemistry of these nonheme diiron enzymes.[11,12]

The study of synthetic diiron(III)−peroxo intermediates[13] has greatly enhanced our understanding of the corresponding species in proteins. Three diiron(III)−peroxo complexes have been crystallographically characterized,[14−16] and the structure of a fourth one has been deduced by EXAFS analysis.[17] While detailed thermodynamic[18] and kinetic[19−23] studies on dioxygen binding to some diiron(II) complexes have been reported, the factors that affect subsequent decomposition of these peroxo complexes and their oxidative reactivities with substrates are much less well understood.[24,25] In contrast, detailed studies have been reported of related copper and nickel complexes that generate peroxo intermediates that effect intramolecular ligand oxidation[26,27] and, in some cases, intermolecular oxidation of added substrates.[28−32]

Previously, we reported the generation and characterization of a (μ-1,2-peroxo)diiron(III) complex from the diiron(II) precursor $[Fe_2(HPTP)(O_2CC_6H_5)]X_2$[33] (see Scheme 1).[24] Our initial studies showed that the O_2 adduct of $[Fe_2(HPTP)(O_2CC_6H_5)]^{2+}$ reacted with PPh_3 and 2,4-di-*tert*-butylphenol, unlike its structurally characterized benzimidazole analogue (*N*-Et-HPTB, Scheme 1),[15] which was unreactive toward these substrates. Thus a change from pendant benzimidazoles to pyridines elicits a dramatic change in reactivity. In this paper, we have extended our initial studies to a series of $[Fe^{II}_2(HPTP)]$ complexes bridged by one or two carboxylates. The crystal structures of two of these precursor complexes are reported, as well as kinetic studies for the formation and decay of their O_2 adducts. The reactivities of the O_2 adducts depend on the number of carboxylate bridges present. These differences provide insight into some of the factors that modulate the stability and oxidative power of the (μ-1,2-peroxo)diiron(III) unit in chemistry and biology.

Scheme 1

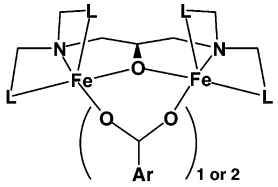

HPTP: L = 2-pyridyl
***N*-Et-HPTB:** L = 1-ethylbenzimidazol-2-yl

$[Fe^{II}_2(HPTP)(O_2CAr)]^{2+}$	$[Fe^{II}_2(HPTP)(O_2CAr)_2]^{+}$
1, Ar = C_6H_5	**6**, Ar = C_6H_5
2, Ar = *p*-Cl-C_6H_4	**7**, Ar = *p*-Cl-C_6H_4
3, Ar = C_6F_5	**8**, Ar = *p*-C_6H_5-C_6H_4
4, Ar = *p*-MeO-C_6H_4	**9**, Ar = *p*-MeO-C_6H_4
5, Ar = *p*-MeC_6H_4	**10**, Ar = *p*-MeC_6H_4

Experimental Section

Synthesis. The dinucleating ligand H−HPTP was synthesized following the published procedure.[34] The diiron(II) complexes **1**−**5** were prepared following the published procedure for $[Fe^{II}_2(HPTP)(O_2CC_6H_5)](BPh_4)_2$[24] by combining 2 equiv of $Fe(O_3SCF_3)_2 \cdot 2CH_3CN$, 1 equiv of H−HPTP·4$HClO_4$, 1 equiv of ArCOOH, and 6 equiv of Et_3N in methanol, stirring for 30 min, and then precipitating the complexes with the addition of 2 equiv of $NaBPh_4$. Recrystallization from CH_3CN/ether afforded analytically pure complexes. Tetramethylammonium salts of benzoic acids were prepared by neutralizing the acid using $(Me_4N)OH$ in MeOH/H_2O and subsequently removing the solvent under reduced pressure. The purity of the salts was checked using ^1H NMR.

$[Fe^{II}_2(HPTP)(O_2CC_6H_5)](BPh_4)_2$. Anal. for (**1**)$(BPh_4)_2$ or $C_{82}H_{74}B_2Fe_2N_6O_3$, Calcd (Found): C, 74.34 (74.35); H, 5.63 (5.73); N, 6.34 (6.29). λ_{max} (ϵ, M^{-1} cm^{-1}) in MeCN: 326 (2200), 400 sh.

$[Fe^{II}_2(HPTP)(O_2CC_6H_4$-*p*-Cl$)](BPh_4)_2$. Anal. for (**2**)$(BPh_4)_2$ or$C_{82}H_{73}B_2ClFe_2N_6O_3$, Calcd (Found): C, 72.46 (72.45); H, 5.41 (5.48); N, 6.18 (6.31). λ_{max} (ϵ, M^{-1} cm^{-1}) in MeCN: 324 (2400), 375 sh.

(10) Shu, L.; Nesheim, J. C.; Kauffmann, K.; Münck, E.; Lipscomb, J. D.; Que, L., Jr. *Science* **1997**, *275*, 515−518.
(11) Que, L., Jr. *J. Chem. Soc., Dalton Trans.* **1997**, 3933−3940.
(12) Du Bois, J.; Mizoguchi, T. J.; Lippard, S. J. *Coord. Chem. Rev.* **2000**, *200*−*202*, 443−485.
(13) Girerd, J.-J.; Banse, F.; Simaan, A. J. *Struct. Bonding* **2000**, *97*, 143−177.
(14) Ookubo, T.; Sugimoto, H.; Nagayama, T.; Masuda, H.; Sato, T.; Tanaka, K.; Maeda, Y.; Okawa, H.; Hayashi, Y.; Uehara, A.; Suzuki, M. *J. Am. Chem. Soc.* **1996**, *118*, 701−702.
(15) Dong, Y.; Yan, S.; Young, V. G., Jr.; Que, L., Jr. *Angew. Chem., Int. Ed. Engl.* **1996**, *35*, 618−620.
(16) Kim, K.; Lippard, S. J. *J. Am. Chem. Soc.* **1996**, *118*, 4914−4915.
(17) Dong, Y.; Zang, Y.; Shu, L.; Wilkinson, E. C.; Que, L., Jr.; Kauffmann, K.; Münck, E. *J. Am. Chem. Soc.* **1997**, *119*, 12683−12684.
(18) Sugimoto, H.; Nagayama, T.; Maruyama, S.; Fujinami, S.; Yasuda, Y.; Suzuki, M.; Uehara, A. *Bull. Chem. Soc. Jpn.* **1998**, *71*, 2267−2279.
(19) (a) Feig, A. L.; Becker, M.; Schindler, S.; van Eldik, R.; Lippard, S. J. *Inorg. Chem.* **1996**, *35*, 2590−2601. (b) Feig, A. L.; Becker, M.; Schindler, S.; van Eldik, R.; Lippard, S. J. *Inorg. Chem.* **2003**, *42*, 3704
(20) Feig, A. L.; Masschelein, Z.; Bakac, A.; Lippard, S. J. *J. Am. Chem. Soc.* **1997**, *119*, 334−342.
(21) LeCloux, D. D.; Barrios, A. M.; Mizoguchi, T. J.; Lippard, S. J. *J. Am. Chem. Soc.* **1998**, *120*, 9001−9014.
(22) Kryatov, S. V.; Rybak-Akimova, E. V.; MacMurdo, V. L.; Que, L., Jr. *Inorg. Chem.* **2001**, *40*, 2220−2228.
(23) Chavez, F. A.; Ho, R. Y. N.; Pink, M.; Young, V. G., Jr.; Kryatov, S. V.; Rybak-Akimova, E. V.; Andres, H. P.; Münck, E.; Que, L., Jr.; Tolman, W. B. *Angew. Chem., Int. Ed.* **2002**, 149−152.
(24) Dong, Y.; Ménage, S.; Brennan, B. A.; Elgren, T. E.; Jang, H. G.; Pearce, L. L.; Que, L., Jr. *J. Am. Chem. Soc.* **1993**, *115*, 1851−1859.
(25) LeCloux, D. D.; Barrios, A. M.; Lippard, S. J. *Bioorg. Med. Chem.* **1999**, *7*, 763−772.
(26) Tolman, W. B. *Acc. Chem. Res.* **1997**, *30*, 227−237.
(27) Que, L., Jr.; Tolman, W. B. *Angew. Chem., Int. Ed.* **2002**, *41*, 1114−1137.
(28) Mahadevan, V.; DuBois, J. L.; Hedman, B.; Hodgson, K. O.; Stack, T. D. P. *J. Am. Chem. Soc.* **1999**, *121*, 5583−5584.
(29) Mahadevan, V.; Henson, M. J.; Solomon, E. I.; Stack, T. D. P. *J. Am. Chem. Soc.* **2000**, *122*, 10249−10250.
(30) Taki, M.; Itoh, S.; Fukuzumi, S. *J. Am. Chem. Soc.* **2001**, *123*, 6203−6204.
(31) Taki, M.; Itoh, S.; Fukuzumi, S. *J. Am. Chem. Soc.* **2002**, *124*, 998−1002.
(32) Zhang, C. X.; Liang, H.-C.; Kim, E.-i.; Shearer, J.; Helton, M. E.; Kim, E.; Kaderli, S.; Incarvito, C. D.; Zuberbuhler, A. D.; Rheingold, A. L.; Karlin, K. D. *J. Am. Chem. Soc.* **2003**, *125*, 634−635.

(33) Abbreviations used: BIPhMe = 2,2′-bis(1-methylimidazolyl)phenylmethoxymethane; BPMP = 2,6-bis[[bis(2-pyridylmethyl)amino]methyl]-4-methylphenolate; Δ9D = stearoyl acyl carrier protein Δ^9-desaturase; HPTP = anion of *N*,*N*,*N*′,*N*′-tetrakis(2-pyridylmethyl)-2-hydroxy-1,3-diaminopropane; Me_3TACN = 1,4,7-trimethyl-1,4,7-triazacyclononane; 6-Me_4-HPTP = anion of *N*,*N*,*N*′,*N*′-tetrakis(6-methyl-2-pyridylmethyl)-2-hydroxy-1,3-diaminopropane; MMO = methane monooxygenase, *N*-Et-HPTB = anion of *N*,*N*,*N*′,*N*′-tetrakis[(*N*-ethyl-2-benzimidazolyl)methyl]-2-hydroxy-1,3-diaminopropane; RNR, ribonucleotide reductase; Tp^{iPr2} = hydrotris(3,5-diisopropylpyrazolyl)borate anion; TPPDO = anion of *N*,*N*,*N*′,*N*′-tetrakis(6-pivalamido-2-pyridylmethyl)-2-hydroxy-1,3-diaminopropane.

(34) McKee, V.; Zvagulis, M.; Dagdigian, J. V.; Patch, M. G.; Reed, C. A. *J. Am. Chem. Soc.* **1984**, *106*, 4765−4772.

[Fe^{II}_2(HPTP)($O_2CC_6F_5$)](BPh$_4$)$_2$. Anal. for (**3**)(BPh_4)$_2$ or $C_{82}H_{69}B_2F_5Fe_2N_6O_3$, Calcd (Found): C, 69.61 (69.53); H, 4.91 (4.91); N, 5.94 (5.97). λ_{max} (ϵ, M^{-1} cm^{-1}) in MeCN: 323 (1700), 375 sh.

[Fe^{II}_2(HPTP)($O_2CC_6H_4$-*p*-OMe)](BPh$_4$)$_2$. Anal. for (**4**)(BPh_4)$_2$·$3H_2O$ or $C_{83}H_{83}B_2Fe_2N_6O_7$, Calcd (Found): C, 70.71 (70.45); H, 5.96 (5.79); N, 5.93 (6.02). λ_{max} (ϵ, M^{-1} cm^{-1}) in MeCN: 338 (2300), 450 sh.

[Fe^{II}_2(HPTP)($O_2CC_6H_4$-*p*-Me)](BPh$_4$)$_2$. Anal. for (**5**)(BPh_4)$_2$·$2H_2O$ or $C_{83}H_{80}B_2Fe_2N_6O_5$, Calcd (Found): C, 72.51 (72.35); H, 5.86 (5.62); N, 6.11 (6.24). λ_{max} (ϵ, M^{-1} cm^{-1}) in MeCN: 324 (2500), 375 sh.

[Fe^{II}_2(HPTP)($O_2CC_6H_5$)$_2$](BPh$_4$), (6)(BPh$_4$). This complex was synthesized by the addition of a solution of $Me_4N(O_2CC_6H_5)$ (0.024 g, 0.123 mM) in MeCN to a stirred solution of **1** (0.161 g, 0.121 mM) in MeCN. Immediately, the light yellow solution of **1** changed to red, and **6** was precipitated as a red crystalline powder within 10 min. The precipitate was filtered and dried under vacuo (0.118 g, 96%). The complex was recrystallized from CH_2Cl_2 and diethyl ether as red needles. Anal. for (**6**)(BPh_4)$_2$·MeCN·$0.5H_2O$ or $C_{67}H_{63}BFe_2N_7O_{5.5}$, Calcd (Found): C, 68.38 (68.31); H, 5.40 (5.42); N, 8.33 (8.56). λ_{max} (ϵ, M^{-1} cm^{-1}) in CH_2Cl_2 at 298 K: 367 (2600), 480 sh.

[Fe^{II}_2(HPTP)($O_2CC_6H_4$-*p*-Cl)$_2$](BPh$_4$). Anal. for (**7**)(BPh_4)·MeCN·H_2O or $C_{67}H_{62}BCl_2Fe_2N_7O_6$, Calcd (Found): C, 64.14 (64.22); H, 4.98 (4.79); N, 7.81 (7.54); Cl, 5.64 (5.94). λ_{max} (ϵ, M^{-1} cm^{-1}) in CH_2Cl_2 at 233 K: 384 (2000).

[Fe^{II}_2(HPTP)($O_2CC_6H_4$-*p*-C_6H_5)$_2$](BPh$_4$). Anal. for (**8**)(BPh_4)·MeCN·H_2O or $C_{79}H_{72}BFe_2N_7O_6$, Calcd (Found): C, 70.92 (70.55); H, 5.42 (5.34); N, 7.33 (7.15). λ_{max} (ϵ, M^{-1} cm^{-1}) in CH_2Cl_2 at 233 K: 364 (2300).

[Fe^{II}_2(HPTP)($O_2CC_6H_4$-*p*-Me)$_2$](BPh$_4$). Anal. for (**9**)(BPh_4) or $C_{67}H_{63}BFe_2N_6O_5$, Calcd. (Found): C, 69.69 (69.43); H, 5.50 (5.51); N, 7.28 (7.40). λ_{max} (ϵ, M^{-1} cm^{-1}) in CH_2Cl_2 at 233 K: 360 (2200), 460 sh.

[Fe^{II}_2(HPTP)($O_2CC_6H_4$-*p*-OMe)$_2$](BPh$_4$). Anal. for (**10**)(BPh_4)·2MeCN·$0.5H_2O$ or $C_{71}H_{70}BFe_2N_8O_{7.5}$, Calcd. (Found): C, 66.73 (66.81); H, 5.52 (5.37); N, 8.77 (8.51). λ_{max} (ϵ, M^{-1} cm^{-1}) in CH_2Cl_2 at 233 K: 336 (2500), 464 (1600).

Physical Methods. UV−vis spectra were recorded on a HP 8452A diode array spectrometer. Low-temperature visible spectra were obtained using an immersion dewar equipped with quartz windows. GC analyses were performed with a Perkin-Elmer Autosystem equipped with an Alltech 1701 30 m × 0.25 mm × 0.25 μm capillary column. GC-MS analysis were carried out in a HP-5898 GC equipped with a DB-5 capillary column and a Finnigan MAT 95 mass detector, using NH_3 as ionization gas. NMR spectra were recorded on a Varian VXR 300 spectrophotometer. The ^{1}H NMR spectra were recorded using a 90° pulse with 16K data points. An inversion−recovery pulse sequence (180°−τ−90°−AQ) was used to obtain nonselective proton relaxation times (T_1) with carrier frequencies set at several different positions to ensure the validity of the measurements.

Infrared spectra were obtained from KBr pellets on a Nicolet Avatar 320 FT-IR instrument. The KBr pellet of **6**·O_2 was made within a 3-min period at room temperature after its isolation as a solid sample at −40 °C to minimize its decomposition. Resonance Raman spectra were collected using a backscattering geometry on sample solutions frozen on a coldfinger cooled to 77 K with 568-nm laser excitation (30 mW at the sample) from a Spectra Physics 2030-15 argon ion laser and a 375B CW dye (Rhodamine 6G) laser. Spectra were calibrated with indene and recorded with an Acton AM-506 spectrometer (2400-groove grating) using a Kaiser Optical holographic super-notch filter with a Princeton Instruments liquid N_2-cooled (LN-1100PB) CCD detector with 4 cm^{-1} spectral resolution.

Generation of Peroxo Adducts and Conventional Kinetic Experiments. The peroxo adduct intermediates were generated in an immersion dewar maintained at the appropriate low temperature by bubbling pure oxygen at atmospheric pressure through a CH_2Cl_2/DMSO-d_6 (9:1 v/v) (**1**−**5**) or CH_2Cl_2 (**6**−**10**) solution (approximately 2 mL) of the diiron(II) precursor for 30 s to produce a blue-violet color within seconds. The decomposition of the peroxo intermediates was monitored for at least 5 half-lives, and data were analyzed using the program Specfit (BioLogic Science Instruments, Grenoble, France). As decay started within a few seconds in the presence of substrate, no attempts were made to remove excess O_2. The iron(II) solutions before and after addition of substrate were checked using ^{1}H and ^{31}P NMR and UV−vis spectroscopy, and no evidence was found for substrate binding to the diiron(II) precursor.

Stopped-Flow Studies. All manipulations of **1** and **6** and their solutions were done inside a Vacuum Atmospheres glovebox with argon or using Hamilton airtight syringes. Graduated mixtures of oxygen and nitrogen were prepared using Bel-Art gas flow meters. Saturated solutions of O_2 and graduated O_2−N_2 mixtures were prepared by bubbling the gas through a liquid for 20 min in a cylinder closed with a septum and thermostated at 20 or 25 °C. The solubility of O_2 was accepted to be 5.8 mM in dichloromethane at 20 °C and 8.1 mM in acetonitile at 25 °C.[35,36] Oxygen solubility in dichloromethane−acetonitrile mixtures was estimated by linear interpolation. Kinetic measurements were performed using a Hi-Tech Scientific (Salisbury, Wiltshire, U.K.) SF-43 multimixing anaerobic cryogenic stopped-flow instrument combined with (a) a Hi-Tech Scientific M300 monochromator or (b) a Hi-Tech Scientific Kinetascan diode array rapid scanning unit. No difference in spectral and kinetic data was observed for the monochromator and diode array modes in this study. The mixing cell (1 cm) was maintained to ±0.1 K, and mixing time was 2−3 ms. In all kinetic experiments, a series of 5−7 shots gave standard deviations within 5%, with overall reproducibility within 10%. Data analysis was performed with IS-2 Rapid Kinetics Software (Hi-Tech Scientific) for single-wavelength kinetic traces and with the program Specfit (BioLogic Science Instruments, Grenoble, France) for global fitting of the spectral changes acquired in a diode array mode. Solvent purification proved to be essential for obtaining reproducible data (particularly with complex **1**). Acetonitrile was distilled over CaH_2 followed by another distillation over P_2O_5. Even though the oxygenation reactions were not affected by small quantities of water, this treatment was necessary to remove other impurities. Using anhydrous acetonitrile (Aldrich) or passing the solvent through a column with activated alumina proved insufficient. Dichloromethane (Fisher, >99.9%, GS/MS grade, not stabilized) was additionally treated with basic alumina.

Oxidation of Substrates. A 3 mM solution of the diiron(II) complex in CH_2Cl_2/DMSO-d_6 (9:1 v/v) (**1**) or CH_2Cl_2 (**6**) was transferred, in a drybox, to a 5 mL Schlenk flask which was subsequently sealed with a septum. The Schlenk flask was placed in an acetone bath cooled to −80 °C, and dry O_2 was bubbled through the solution for 10 s. After the appropriate amount of substrate was added via syringe, the complete reaction mixture was purged by three vacuum−argon cycles and maintained at −40 °C with stirring. After 2 h at −40 °C, the acetone bath was removed, and the reaction

(35) Battino, R. In *Solubility Data Series Vol. 7. Oxygen and Ozone*; Battino, R., Ed.; Pergamon: New York, 1981.
(36) Achord, J. M.; Hussey, C. L. *Anal. Chem.* **1980**, *52*, 601−602.

Table 1. Crystallographic Data for (**3**·CH_3CN)$(BPh_4)_2$·CH_3CN and (**6**)(BF_4)·CH_3CN

	(**3**·CH_3CN)$(BPh_4)_2$·CH_3CN	(**6**)(BF_4)·CH_3CN
formula	$C_{86}H_{75}B_2F_5Fe_2N_8O_3$	$C_{67}H_{62}BFe_2N_7O_5$
fw	1496.86	1167.75
cryst color	yellow	reddish brown
T	173(2) K	173(2) K
cryst syst	triclinic	triclinic
space group	$P\bar{1}$	$P\bar{1}$
a (Å)	13.674(5)	9.9497(2)
b (Å)	14.212(6)	16.9298(2)
c (Å)	22.138(9)	17.5250(2)
α (deg)	102.342(7)	80.050(1)
β (deg)	96.252(7)	89.116(1)
γ (deg)	90.270(7)	86.714(1)
V	4176(3) Å^3	2902.80(8) Å^3
Z	2	2
D (calcd)	1.190 cm^{-3}	1.336 g cm^{-3}
μ	4.09 cm^{-1}	5.58 cm^{-1}
R1[a]	0.0465	0.0370
wR2[a]	0.1065	0.0777
GOF on F^2	1.022	1.038

[a] $R1 = \sum||F_o| - |F_c||/\sum|F_o|$ and $wR2 = (\sum[w(F_o^2 - F_c^2)^2]/\sum[wF_o^4])^{1/2}$, where $w = q/\sigma^2(F_o^2) + (aP)^2 + bP$.

mixture was allowed to warm to room temperature. Naphthalene was added as an internal standard, and the products were analyzed by GC. Oxidation products were identified by GC-MS analysis and by comparing their retention time with authentic samples.

Crystallographic Experiments. Data collection and structure solution were conducted at the X-ray Crystallographic Laboratory of the University of Minnesota Chemistry Department. All calculations were performed using SGI INDY R4400-SC or Pentium computers using the SHELXTL V5.0 and V5.10 suite of programs. Crystals of (**3**·CH_3CN)$(BPh_4)_2$·CH_3CN and (**6**)(BF_4)·CH_3CN were placed onto the tips of glass capillaries and mounted on a Bruker SMART system for data collection at 173(2) K. Preliminary sets of cell constants were calculated from reflections harvested from three sets of 20 and 60 frames, respectively. These initial sets of frames were oriented such that orthogonal wedges of reciprocal space were surveyed. Initial orientation matrices were determined from 53 and 570 reflections, respectively. Final cell constants were calculated from a set of 1024 and 14878 reflections, respectively. Additional crystallographic data and refinement information are summarized in Table 1.

For (**3**·CH_3CN)$(BPh_4)_2$·CH_3CN**,** the space group $P\bar{1}$ was determined on the basis of systematic absences and intensity statistics. A direct-methods solution was calculated which afforded positions of most non-hydrogen atoms from the E-map. Full-matrix least-squares/difference Fourier cycles were performed which located the remaining non-hydrogen atoms. All non-hydrogen atoms were refined with anisotropic displacement parameters. All hydrogen atoms were placed in ideal positions and refined as riding atoms with individual (or group if appropriate) isotropic displacement parameters.

Because an unknown amount of disordered solvent was present in the structure, the data set was modified using the program PLATON/SQUEEZE.[37] An investigation of the void space in the structure showed that 116 electrons are located in one major void of approximately 635.1 Å^3. The refinement using the corrected data set improved the overall structure and the R1 value. Some of the given values in the CIF file are known to be incorrect due to the unknown amount of solvent (e.g., F(000), formula, formula weight). Selected bond lengths and angles are listed in Table 2.

(37) Spek, A. L. *PLATON. A multipurpose crystallographic tool*; Utrecht University: Utrecht, The Netherlands, 2002.

Table 2. Selected Bond Lengths (Å) and Bond Angles (deg) for (**3**·CH_3CN)$(BPh_4)_2$·CH_3CN and (**6**)(BF_4)·CH_3CN

(**3**·CH_3CN)$(BPh_4)_2$·CH_3CN		(**6**)(BF_4)·CH_3CN	
Fe1−O1	1.9390(17)	Fe1−O1	1.9906(14)
Fe1−O2	2.0636(18)	Fe1−O2	2.131(2)
Fe1−N4	2.2410(19)	Fe1−O4	2.052(2)
Fe1−N5	2.101(2)	Fe1−N2	2.278(2)
Fe1−N6	2.096(2)	Fe1−N1	2.166(2)
Fe2−O1	2.0061(17)	Fe1−N5	2.185(2)
Fe2−O3	2.0917(18)	Fe2−O1	1.9972(14)
Fe2−N1	2.254(2)	Fe2−O3	2.197(2)
Fe2−N2	2.150(2)	Fe2−O5	2.0585(14)
Fe2−N3	2.175(2)	Fe2−N3	2.256(2)
Fe2−N7	2.218(2)	Fe2−N4	2.159(2)
		Fe2−N6	2.247(2)
Fe1···Fe2	3.47	Fe1···Fe2	3.30
Fe1−O1−Fe2	123.18(8)	Fe1−O1−Fe2	111.74(6)

For (**6**)(BF_4)•CH_3CN, the space group $P\bar{1}$ was determined on the basis of systematic absences and intensity statistics. A Patterson solution was calculated, which provided the positions of the heavy atoms. Several full-matrix least-squares/difference Fourier cycles were performed to locate the remaining non-hydrogen atoms. All non-hydrogen atoms were refined with anisotropic displacement. All hydrogen atoms were found from the difference map and refined for all parameters. The structure was found with one solvent molecule, acetonitrile, per asymmetric unit. Selected bond lengths and angles are listed in Table 2.

Results and Discussion

The monocarboxylate-bridged diiron(II) complexes $[Fe^{II}_2(HPTP)(O_2CAr)](BPh_4)_2$ (**1**−**5**, Scheme 1) were synthesized following the method of Dong et al.,[24] while their bis(carboxylate) analogues $[Fe^{II}_2(HPTP)(O_2CAr)_2](BPh_4)$ (**6**−**10**, Scheme 1) were obtained by reaction of the corresponding monocarboxylate complex with 1 equiv of $(Me_4N)(O_2CAr)$ in acetonitrile. Yields were somewhat dependent on the nature of the carboxylate, ranging from 34% for Ar = p-$OMeC_6H_4$ to practically quantitative for Ar = C_6H_5. These complexes serve as precursors to metastable dioxygen adducts that are the focus of this investigation.

Crystal Structures of (3·CH_3CN)$(BPh_4)_2$ and 6(BF_4). ORTEP plots based on the solid state structures of the cations of (**3**·CH_3CN)$(BPh_4)_2$ and **6**(BF_4) are shown in Figure 1. For both complexes, the diiron(II) center is bridged by the alkoxo oxygen atom, and each iron is facially capped by the tridentate bis(2-pyridylmethyl)amine moieties on either end of the 2-hydroxypropane backbone of the HPTP ligand. For **3**, there is one bidentate carboxylate bridge, which coordinates *trans* to the amine nitrogen of each iron (Figure 1a). Interestingly, the two iron atoms have different coordination geometries. Fe1 is trigonal bipyramidal ($\tau = 0.86$), with the amine nitrogen and the carboxylate oxygen defining the trigonal axis. Fe2 is six-coordinate but has a similar ligand arrangement as Fe1 except that the trigonal plane has expanded to accommodate an acetonitrile ligand trans to one of the pyridines. Complex cation **6** has two carboxylate bridges, and each iron atom is six-coordinate (Figure 1b). Although there is no crystallographically imposed symmetry, the molecule has approximate C_s symmetry with a mirror plane passing perpendicular to the Fe−Fe vector. One benzoate coordinates *trans* to the amine nitrogen atoms of

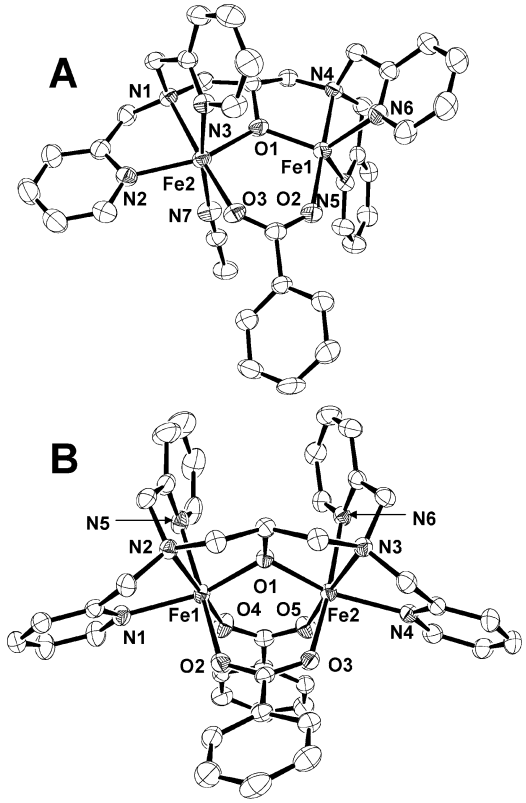

Figure 1. ORTEP plots of (A) cation of **3**, $[Fe^{II}_2(HPTP)(O_2CC_6F_5)(MeCN)]^{2+}$, and (B) the cation of **6**, $[Fe^{II}_2(HPTP)(O_2CC_6H_5)_2]^{+}$, showing 50% probability ellipsoids. Hydrogen and fluorine atoms have been omitted for clarity.

HPTP, as in **3**, while the second benzoate binds *trans* to two of the pyridine rings.

Metal−ligand bond lengths for **3** and **6** listed in Table 2 are characteristic of high spin Fe^{II} complexes. For **3**, the metal−ligand distances for 5-coordinate Fe1 are not surprisingly shorter than those for 6-coordinate Fe2. For example, the average $Fe-N_{py}$ distance is 2.10 Å for Fe1 and 2.16 Å for Fe2. For **6**, both iron ions are 6-coordinate, and the average $Fe-N_{py}$ distance is 2.19 Å, slightly longer than that for the 6-coordinate Fe2 of **3**. More interesting are the two carboxylate bridges, which are distinct from each other. The carboxylate bridge *trans* to the amine nitrogens has an average Fe−O bond (Fe1−O2 and Fe2−O3) of 2.06 Å, comparable to that for **3** (2.08 Å), but the other carboxylate has much longer Fe−O bonds (Fe1−O4 and Fe2−O5), averaging 2.16 Å, suggesting that this carboxylate is more weakly bound. Conversion of **3** to **6** by the introduction of a second carboxylate group results in the closing of the Fe−O−Fe angle from 123° to 112° and a shortening of the Fe−Fe distance from 3.47 to 3.30 Å. As shown in Table 3, these changes are mirrored in the structural differences between other complexes with $[Fe_2(\mu\text{-OR})]$ cores having one or two carboxylate bridges.

Physical Properties of Diiron(II) Complexes. Complexes **1**−**10** are air-sensitive solids. The UV−vis spectra of monocarboxylate complexes **1**−**5** in acetonitrile show no significant absorption in the visible region and intense features in the UV region at $\lambda_{max} = 323-338$ nm ($\epsilon = 1700-2500$ M^{-1} cm^{-1}) arising from iron(II)-to-pyridine charge transfer transitions. Likewise, the UV−vis spectra of the dicarboxylate complexes **6**−**10** in CH_2Cl_2 exhibit an absorption at 335−385 nm ($\epsilon = 2000-2800$ M^{-1} cm^{-1}); the red shift of the MLCT transition is attributed to the presence of the second carboxylate, which diminishes the Lewis acidity of the metal center (Figure 2).

Figure 3 shows the ^1H NMR spectra of **1** and **6**, which are representative of mono- and dicarboxylate complexes, respectively. The ^1H NMR spectra of the complexes show well-resolved, relatively sharp signals that span over 220 ppm in chemical shift. The high resolution and the relatively narrow widths of the signals observed in the spectra are typical of high spin Fe(II) complexes and are similar to those of previously described structurally related diiron(II) complexes.[24,43] The chemical shifts for all 10 complexes are listed in Table S1; most of these can be assigned by their T_1 values and a comparison of the spectra of related complexes. The geminal proton to the alkoxide bridge is readily assigned on the basis of its single-proton integration, short T_1, and large shift due to its proximity to the metal centers. Most, if not all, of the methylene protons appear as well-resolved signals that integrate as two protons each. Since the CH_2 groups are in five-membered metal−chelate rings, the protons comprising each geminal pair can be designated as axial or equatorial and are affected differently by the paramagnetic centers.[43] Thus, the appearance of six distinct resonances demonstrates that the two halves of the dinucleating ligand are magnetically equivalent on the NMR time scale. This notion is also supported by the number of pyridyl resonances observed. A comparison of the spectra of **1**, **2**, and **3** allows the assignment of the aromatic proton signals arising from the carboxylate. Finally, the signals of the different protons in the pyridine ring can be identified on the basis of the dramatic difference in their respective relaxation times.

Generation and Characterization of the Dioxygen Adducts. The monocarboxylate bridged diiron(II) complexes **1**−**5** react with O_2 in CH_2Cl_2/DMSO (9:1 v/v) to generate deep purple species, which are stable only for minutes at low temperature. These O_2 adducts **1**·O_2−**5**·O_2 are best described as diiron(III)−peroxo complexes on the basis of their spectroscopic properties and comparisons with related complexes. The O_2 adducts exhibit one intense and broad visible absorption band with $\lambda_{max} = 573-580$ nm ($\epsilon = 2100-2800$ M^{-1} cm^{-1}) (Table S2). As for previously reported diiron(III) peroxo complexes,[24] this chromophore

(38) (a) Hayashi, Y.; Kayatani, T.; Sugimoto, H.; Suzuki, M.; Inomata, K.; Uehara, A.; Mizutani, Y.; Kitagawa, T.; Maeda, Y. *J. Am. Chem. Soc.* **1995**, *117*, 11220−11229. (b) Arii, H.; Nagatomo, S.; Kitagawa, T.; Miwa, T.; Jitsukawa, K.; Einaga, H.; Masuda, H. *J. Inorg. Biochem.* **2000**, *82*, 153−162.
(39) Kitajima, N.; Tamura, N.; Tanaka, M.; Moro-oka, Y. *Inorg. Chem.* **1992**, *31*, 3342−3343.
(40) Hartman, J. R.; Rardin, R. L.; Chaudhuri, P.; Pohl, K.; Wieghardt, K.; Nuber, B.; Weiss, J.; Papaefthymiou, G. C.; Frankel, R. B.; Lippard, S. J. *J. Am. Chem. Soc.* **1987**, *109*, 7387−7396.
(41) Borovik, A. S.; Hendrich, M. P.; Holman, T. R.; Que, L., Jr.; Papaefthymiou, V.; Münck, E. *J. Am. Chem. Soc.* **1990**, *112*, 6031−6038.
(42) Rardin, R. L.; Tolman, W. B.; Lippard, S. J. *New J. Chem.* **1991**, *15*, 417−430.
(43) Ming, L.-J.; Jang, H. G.; Que, L., Jr. *Inorg. Chem.* **1992**, *31*, 359−364.

Table 3. Structural Parameters of Complexes with $[Fe^{II}_2(L)(\mu\text{-}OR)(O_2CR')_x]$ Cores

diiron(II) complex[a]	R	x	Fe−μ-OR (av), Å	Fe−O−Fe, deg	Fe···Fe, Å	ref
3	alkyl	1	1.97	123.18(8)	3.47	*b*
6	alkyl	2	1.9939(10)	111.74(6)	3.30	*b*
$[Fe^{II}_2(N\text{-Et-HPTB})(OBz)]^{2+}$	alkyl	1	1.97	124.0(3)	3.473(7)	24
$[Fe^{II}_2(6\text{-Me}_4\text{−HPTP})(OBz)]^{2+}$	alkyl	1	2.02	131.2(1)	3.684(1)	38a
$[Fe^{II}_2(TPPDO)(O_2CC_6H_4\text{-4-Cl})]^{2+}$	alkyl	1	2.07		3.732(1)	38b
$[Fe^{II}_2(OH)(Tp^{iPr2})_2(OBz)]$	H	1	1.98	137.0(3)	3.681(3)	39
$[Fe^{II}_2(Me_3TACN)_2(OH)(OAc)_2]^+$	H	2	1.987(8)	113.2(2)	3.32(1)	40
$[Fe^{II}_2(BPMP)(OPr)_2]^+$	aryl	2	2.057(1)	108.93(6)	3.348(2)	41
$[Fe^{II}_2(O_2CH)_4(BIPhMe)_2]$	formyl	2	2.142(1)	113.0(1)	3.573(8)	42

[a] For abbreviations used, see footnote 33. [b] This work.

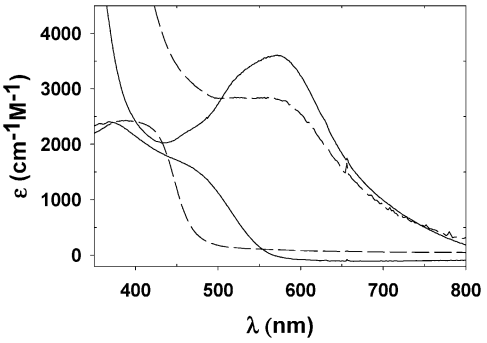

Figure 2. UV−vis spectra, at −60 °C, of **1** (- - -, left) and **1**·O_2 (- - -, right) in CH_2Cl_2/DMSO (9:1 v/v) and of **6** (—, left) and **6**·O_2 (—, right) in CH_2Cl_2.

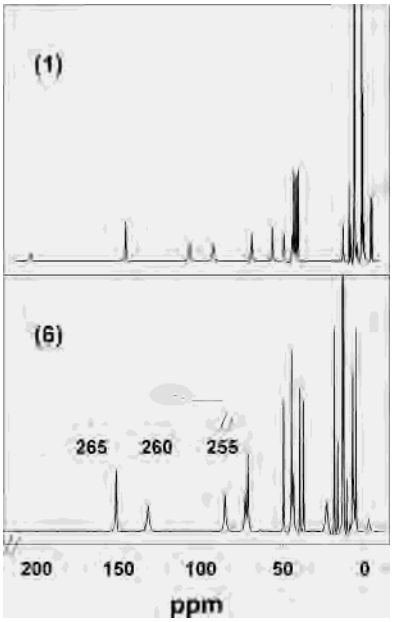

Figure 3. ^{1}H NMR spectra of **1** in CD_3CN and **6** in CD_2Cl_2 at room temperature.

is assigned to a peroxo-to-Fe(III) charge transfer transition. Consistent with this assignment, resonance Raman spectra of **1**·O_2 with 568 nm laser excitation shows a Fermi doublet at 453 and 481 cm^{-1} assigned to ν(Fe−O), and another Fermi doublet at 877 and 893 cm^{-1} assigned to ν(O−O).

The formation of **1**·O_2−**5**·O_2 cannot be detected by conventional spectrophotometry in the absence of DMSO[38,44] under our low temperature conditions.[24] However, a transient

Scheme 2

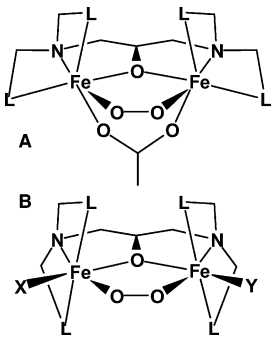

1·O_2 adduct has been observed in the absence of DMSO under stopped-flow conditions[19] and presumably has the structure depicted in Scheme 2A. So the presence of DMSO must stabilize the peroxo complex, allowing its concentration to build up for characterization without the need for fast detection techniques. The addition of $OPPh_3$ has a similar effect on the stability of the O_2 adduct. Indeed, the addition of $OPPh_3$ to the O_2 adduct of the corresponding *N*-Et-HPTB complex stabilized it sufficiently to allow diffraction quality crystals to be obtained and resulted in its crystallographic characterization.[15] That structure revealed a (μ-alkoxo)-(μ-1,2-peroxo)diiron(III) complex in which the carboxylate bridge had been displaced by two molecules of $OPPh_3$ (Scheme 2B, X = Y = Ph_3PO). A similar scenario may be considered for the HPTP complexes in this study (Scheme 2B, X = Y = DMSO), but the observation that the λ_{max}'s of the dioxygen adducts in the presence of DMSO remain sensitive to the basicity of the carboxylate group (Table S2) suggests that the latter is still coordinated to the iron after the oxygen binding step. Thus, we propose that only one DMSO molecule coordinates to the adduct, converting the carboxylate bridge into a terminal ligand on one iron (Scheme 2B, X = OOCR, Y = DMSO).

In contrast, O_2 adducts of **6**−**10** in CH_2Cl_2 (λ_{max} = 572−575 nm; ϵ = 3000−3500 M^{-1} cm^{-1}) (Table S2) remain indefinitely stable at −60 °C. The second carboxylate group, like DMSO, stabilizes the adduct, suggesting that both molecules may act in a similar mode. Raman spectra of **6**·O_2, obtained with 568.2 nm laser excitation, show resonance enhanced features at 456, 482, 888, and 902 cm^{-1}, which are quite similar to those observed for **1**·O_2. This similarity in ν(Fe−O) and ν(O−O) values for **1**·O_2 and **6**·O_2 suggests that the peroxide is coordinated in a similar fashion in both complexes and that the Fe−O and O−O bond strengths and the geometry of the Fe−O−O−Fe unit are not significantly

(44) Hayashi, Y.; Suzuki, M.; Uehara, A.; Mizutani, Y.; Kitagawa, T. *Chem. Lett.* **1992**, 91−94.

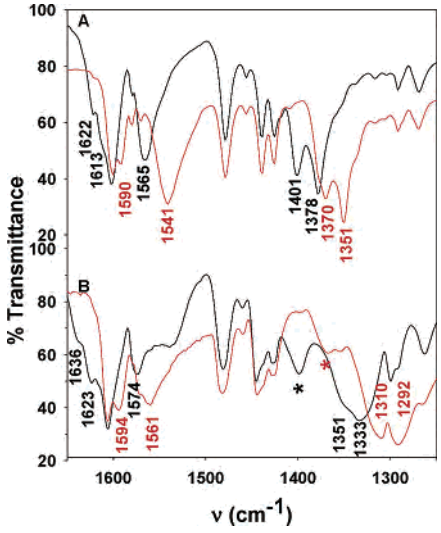

Figure 4. IR spectra of (A) **6** and (B) **6**·O_2. Black spectra correspond to samples with natural abundance benzoate, and red spectra correspond to samples with benzoate ^{13}C-labeled at the carboxylate group. Asterisks designate peaks arising from decayed product.

Table 4. Comparison of Carboxylate Stretches (cm^{-1}) for **6** and **6**·O_2

	asym		sym		
sample	ν_{COO}	ν_{COO}	ν_{COO}	ν_{COO}	$\Delta\nu$(asym − sym)
6 ($O_2^{n.a.}$CAr)	1622, 1613	1565	1401	1378	216, 187
6 (O_2^{13}CAr)	1590	1541	1370	1351	220, 190
6·O_2 ($O_2^{n.a.}$CAr)	1636, 1623	1574	1351	1333	279, 241
6·O_2 (O_2^{13}CAr)	1594	1561	1310	1292	284, 269
$Me_4N^+C_6H_5^{n.a.}COO^-$	1553		1399		154
$Me_4N^+C_6H_5{}^{13}COO^-$	1516		1368		148

affected by the introduction of the second carboxylate group.[45]

FT-IR spectroscopy was used to show that the carboxylate bridges of **6** became monodentate upon formation of the peroxo intermediate. Carboxylates exhibit characteristic symmetric and asymmetric stretching modes, the separation ($\Delta\nu$) of which is indicative of the binding mode of the carboxylate.[46] The $\Delta\nu$ value for a bidentate carboxylate bridge should be comparable to that of the ionic carboxylate but smaller than that for a monodentate carboxylate. The IR spectrum of a KBr pellet of **6** shows features at 1622, 1613, 1565, 1401, and 1378 cm^{-1}, which shift to 1590, 1541, 1370, and 1351 cm^{-1} with ^{13}C labeling of the carboxylate carbon on the benzoate group (Figure 4). The presence of an intense ^{13}C-insensitive feature at 1602 cm^{-1} and the observation of three ^{13}C-sensitive peaks in the ν_{asym} region complicate the interpretation of the natural abundance data. However, the ^{13}C data are more straightforward to analyze, affording $\Delta\nu$ values of 220 and 190 cm^{-1} for **6**. For comparison, (Me_4N)($O_2{}^{13}CC_6H_5$) has features at 1516 and 1368 cm^{-1}, giving a $\Delta\nu$ of 148 cm^{-1} (Table 4). Thus, the $\Delta\nu$ values observed for **6** are consistent with the presence of bridging carboxylates. The IR spectrum of **6**·O_2, on the other hand, shows features at 1636, 1623, 1574, 1351, and 1333 cm^{-1}, which shift to 1594, 1561, 1310, and 1292 cm^{-1} in the ^{13}C isotopomer. Compared to its precursor, the O_2 adduct exhibits ν_{asym} features upshifted by 10−15 cm^{-1} and ν_{sym} features downshifted by about 50 cm^{-1}, leading to a dramatic increase in the $\Delta\nu$ values (284 and 269 cm^{-1}). These results unequivocally demonstrate that the carboxylates of **6** have become monodentate upon formation of the O_2 adduct (Scheme 2B, X = Y = $^-$OOCR).

Oxygenation Kinetics. Choice of Solvents and Additives. A detailed kinetic analysis has been performed on the oxygenation of **1** and **6**. Oxygenation kinetics data were previously reported in propionitrile for **1** and related monocarboxylate-bridged complexes.[19] Although no substantial difference between oxygenation rates in propionitrile and acetonitrile was expected, control experiments on oxygen binding to **1** in acetonitrile were performed. Complex **6** was insoluble in polar solvents but soluble in chlorinated hydrocarbons, making noncoordinating CH_2Cl_2 the solvent of choice. For direct comparisons of **1** and **6**, oxygenation in CH_3CN/CH_2Cl_2 mixtures was also investigated. Peroxo intermediates derived from **1** were greatly stabilized by the addition of oxygen donors (DMSO or Ph_3PO), which coordinate to the metal centers in both the diiron(II) complexes and corresponding diiron(III) peroxo adducts.[15,24] These additives however could retard the oxygenation rates by blocking vacant iron(II) coordination sites in **1**. Direct measurements were needed in order to determine the influence of oxygen donors on the oxygenation rates.

Kinetic measurements were performed under pseudo-first-order conditions (large excess of dioxygen with respect to diiron complex) over the temperature range from −40 to 0 °C in CH_3CN, and from −80 to 0 °C for CH_2Cl_2. As expected, the oxygenation of **1** in CH_3CN or CH_3CN/CH_2Cl_2 mixtures proceeded similarly to oxygenation of **1** in propionitrile,[19] with rapid accumulation of the peroxo species (over ca. 200 ms at −40 °C, CH_3CN) immediately followed by its decomposition, but reproducible kinetic parameters could be obtained only in doubly distilled (over CaH_2 and over P_2O_5) CH_3CN. The oxygenation of **1** in the presence of oxygen donors (DMSO and Ph_3PO) and of **6** proceeded as essentially one-exponential reactions on the stopped-flow time scale, as the decomposition of peroxo adducts was much slower than oxygen binding to diiron(II) complexes **1** and **6** (Figure 5). Spectral changes upon oxygenation observed by stopped-flow spectrophotometry were identical to those obtained by regular spectrophotometry in the "batch" experiments and corresponded to clean peroxide formation in the first stage of the reactions.

Rate Law and Activation Parameters. The observed pseudo-first-order rate constants for peroxo complex formation were independent of the concentration of the diiron(II) complexes but increased linearly with dioxygen concentration (Figure 6). Consequently, the oxygenation of complexes **1** and **6** is a second-order process (first-order in diiron(II) complex, and first-order in O_2):

$$v = k_{obs}[Fe_2] = k[O_2][Fe_2]$$

The rate law was identical for all reactions studied (Table

(45) Brunold, T. C.; Tamura, N.; Kitajima, M.; Moro-oka, Y.; Solomon, E. I. *J. Am. Chem. Soc.* **1998**, *120*, 5674−5690.
(46) Nakamoto, K. *Infrared and Raman Spectra of Inorganic and Coordination Compounds*, 4th ed.; John Wiley: New York, 1986.

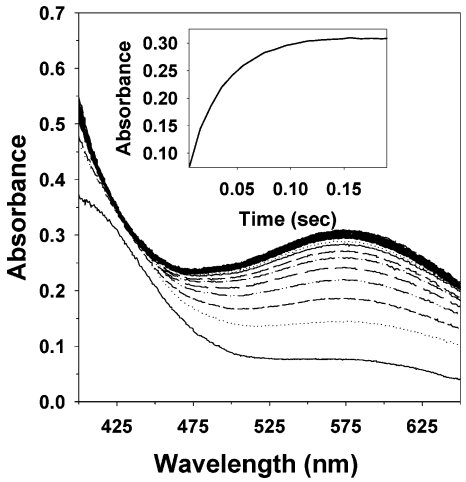

Figure 5. Spectral changes upon oxygenation of **1** in CH_3CN at −40 °C. Individual spectra were collected at 10.0 ms intervals. [**1**] = 2.23 × 10^{-4} M, [O_2] = 4.05 × 10^{-3} M. The inset shows a kinetic trace at 573 nm that corresponds to a pseudo-first-order formation of **1**·O_2 (k_{obs} = 30.5 s^{-1}).

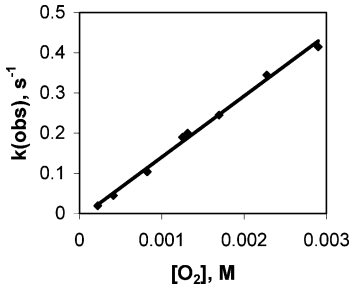

Figure 6. Plot of the observed pseudo-first-order rate constant, *k*(obs), vs dioxygen concentration for the oxygenation of **6** in CH_2Cl_2. Temperature −20.9 °C, initial concentration of **6** is 4.58 × 10^{-5} M.

5) and did not change with temperature; the oxygenation of **6** in methylene chloride remained a second-order process even at −80 °C. Activation parameters of the oxygenation reactions were determined from linear Arrhenius and Eyring plots (Figure 7, Table 5). Small activation enthalpies ($\Delta H^{\ddagger}$ = 8−19 kJ/mol) and large negative activation entropies ($\Delta S^{\ddagger}$ = −140 to −90 J/K mol) are typical of associative reactions.[47] Thus, ligand dissociation to generate a binding site is facile and cannot be the rate-limiting step in the oxygenation of any of the complexes studied in this work. For example, in the case of **6**, a carboxylate shift[42] from a bridging bidentate mode to a terminal monodentate mode is quite plausible and suggested by the longer Fe1−O2 and Fe2−O3 bridging carboxylate distances observed in its crystal structure (Table 2).

While oxygen binding to **1** and **6** under different conditions shares the same rate-limiting step, the oxygenation rates are somewhat sensitive to the nature of additional ligands and solvents (Figure 7 and Table 5). Oxygen binding to **6** is almost an order of magnitude slower than to its coordinatively unsaturated counterpart **1** in the same solvent mixture (1:1 CH_3CN/CH_2Cl_2). Similarly, oxygenation of **1** in CH_3CN is retarded by a factor of 2 in the presence of 10 equiv of Ph_3PO, and by a factor of 3 in the presence of 10% DMSO. These effects, however, are relatively small as compared to the dramatic increase observed in the stability of the peroxo adducts. Thus, coordination of labile oxygen donors is not detrimental for the oxygenation step and highly effective for suppressing peroxide decomposition pathways. The oxygenation of the diiron(II) complexes with HPTP is much faster than the oxygenation of a six-coordinate, sterically hindered $[Fe_2(\mu\text{-}OH)_2(6\text{-}Me_3\text{-}TPA)_2]^{2+}$ complex investigated previously.[22] These results suggest that the HPTP scaffold does not block access of O_2 to the diiron(II) center and allows for rapid and efficient oxygenation.

The oxygenation rates of diiron(II) HPTP complexes depend on the polarity of the solvent (Table 5). For **1**, diiron(III)−peroxo formation is fastest in CH_3CN and 7-fold slower in proprionitrile.[19] Similarly for **6**, the rate is an order of magnitude faster in 1:1 CH_2Cl_2/CH_3CN than in CH_2Cl_2 alone. The possible coordination of CH_3CN to the metal center(s) as the rationale for the rate acceleration observed for **6** can be discarded, as the presence of 2.5 vol % CH_3CN in CH_2Cl_2 ([CH_3CN]/[**6**] ∼ 1000) does not change the oxygenation rate as compared to pure CH_2Cl_2, but larger volume fractions of CH_3CN in CH_2Cl_2 (up to 50 vol %) do lead to substantially faster (up to 10-fold) oxygenation rates (Table 5). The increase in oxygen binding rates with an increase in solvent polarity supports a polar transition state for the oxygenation process, consistent with the notion that O_2 coordination to iron(II) is accompanied by electron transfer.

Oxygen binding to diiron(II) HPTP complexes studied in this work is a low-barrier process, with an activation enthalpy of only 8−20 kJ/mol (Table 5). The differences in reaction rates originate primarily from the differences in the activation entropies, which become more unfavorable for coordinatively saturated species, so steric effects are responsible for the differences in oxygenation rates. This pattern of small activation enthalpies and large negative activation entropies is commonly found for the association of O_2 and a reduced metal center when formation of a metal−superoxo adduct is believed to be the rate-limiting step. Examples include myoglobin ($\Delta H^{\ddagger}$ = 21 kJ mol^{-1}) and monomeric hemoglobin ($\Delta H^{\ddagger}$ = 24 kJ mol^{-1}),[50,51] as well as dicopper(I) complexes of dinucleating ligands related to HPTP.[52] An extreme example is the slow oxygenation of $[Fe_2(OH)_2(6\text{-}Me_3TPA)_2]^{2+}$, where the bulky ligand prevented easy access of the O_2 molecule to the diiron(II) center, giving rise to a large negative activation entropy.[22] It can be concluded that a delicate balance is required in designing dinuclear iron complexes for oxygen binding and activation. On one hand, steric protection of the metal center is necessary to prevent the

(47) Tobe, M. L.; Burgess, J. *Inorganic Reaction Mechanisms*; Longman: London, 1999.

(48) Valentine, A. M.; Stahl, S. S.; Lippard, S. J. *J. Am. Chem. Soc.* **1999**, *121*, 3876−3887.

(49) Broadwater, J. A.; Achim, C.; Münck, E.; Fox, B. G. *Biochemistry* **1999**, 12197−12204.

(50) Warburton, P. R.; Busch, D. H. In *Perspectives on Bioinorganic Chemistry*; JAI Press: London, 1993; Vol. 2, pp 1−79.

(51) Wilkins, R. G. In *Oxygen Complexes and Oxygen Activation by Transition Metals*; Martell, A. E., Sawyer, D. T., Eds.; Plenum Press: New York, 1987; pp 49−60.

(52) Karlin, K. D.; Kaderli, S.; Zuberbühler, A. D. *Acc. Chem. Res.* **1997**, *30*, 139−147.

Table 5. Kinetic Parameters for the Oxygenation of **1**, **6**, and Other Diiron(II) Complexes

complex, solvent/additive	k_{obs}, s^{-1} (−40 °C, 100% O_2)	k, $M^{-1}s^{-1}$ (−40 °C)	$\Delta H^{\ddagger}$, kJ/mol	$\Delta S^{\ddagger}$, J/K mol	ref
1, CH_3CH_2CN	4.22(13)	$9.6(3) \times 10^2$	16.5 ± 0.4	-114 ± 2	19
1, CH_3CN	29.4(8)	$7.3(5) \times 10^3$	15.8 ± 4	-101 ± 10	*a*
1, CH_3CN/DMSO (9:1 v/v)	11.4(4)	$2.8(2) \times 10^3$	8.0 ± 3	-143 ± 10	*a*
1, CH_3CN/10 equiv Ph_3PO	18.3(8)	$4.5(3) \times 10^3$	15.9 ± 3	-104 ± 10	*a*
1, CH_3CN/CH_2Cl_2 (1:1 v/v)	18.8(8)	$5.4(4) \times 10^3$	19.0 ± 4	-90 ± 10	*a*
6, CH_2Cl_2	0.195(5)	67(3)	16.7 ± 2	-132 ± 8	*a*
6, CH_3CN/CH_2Cl_2 (1:40 v/v)[b]	0.203	70.0	N/A	N/A	*a*
6, CH_3CN/CH_2Cl_2 (1:10 v/v)[b]	0.250	86.2	N/A	N/A	*a*
6, CH_3CN/CH_2Cl_2 (1:2 v/v)[b]	0.470	162	N/A	N/A	*a*
6, CH_3CN/CH_2Cl_2 (1:1 v/v)	2.04(6)	$5.9(1) \times 10^2$	16.3 ± 4	-120 ± 10	*a*
$[Fe_2(N\text{-Et-HPTB})(OBz)]^{2+}$, CH_3CH_2CN	4.40(2)	103(12)	15.4 ± 0.6	-121 ± 3	19
$[Fe_2(6\text{-}Me_3TPA)_2(\mu\text{-}OH)_2]^{2+}$, CH_2Cl_2	$2.08(15) \times 10^{-3}$	0.66(6)	17 ± 2	-175 ± 20	22
MMOH (H_2O)			92 ± 17	88 ± 42	48
Δ^9D (H_2O)			22	−134	49

[a] This work. [b] Oxygen solutions were prepared in pure CH_2Cl_2.

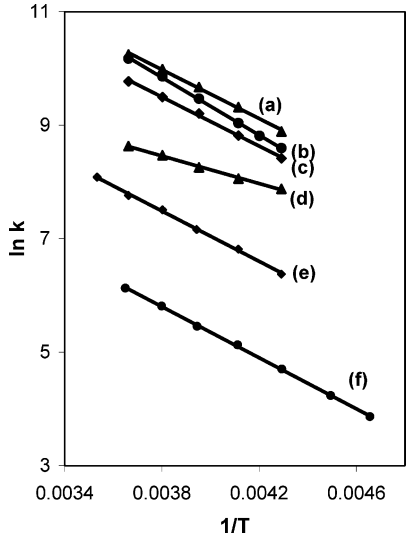

Figure 7. Arrhenius plots for the oxygenation of diiron(II) complexes: (a) **1** in CH_3CN; (b) **1** in CH_3CN/CH_2Cl_2 (1:1 v/v); (c) **1** in CH_3CN in the presence of Ph_3PO (2.5×10^{-4} M solution of **1**, 5×10^{-3} M solution of Ph_3PO); (d) **1** in CH_3CN/DMSO (9:1 v/v); (e) **6** in CH_3CN/CH_2Cl_2 (1:1 v/v); (f) **6** in CH_2Cl_2.

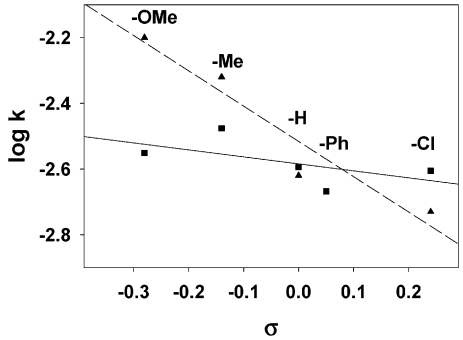

Figure 8. Relationship between the rates of decay (k, s^{-1}) of the peroxo adducts of **1**−**5** (▲) at −40 °C and the peroxo adducts of **6**−**10** at 0 °C (■) versus the Hammett σ value of the para substituent in the bridging benzoate (p-R-$C_6H_4CO_2^-$).

unwanted autoxidation processes; on the other hand, excessive steric hindrance would substantially limit the oxygenation rates.

Peroxide Decomposition Kinetics. The decomposition of the peroxo species **1**·O_2 in propionitrile was previously investigated by stopped-flow methods and reported to be a rapid second-order process.[19] In complete agreement with these previous findings, our stopped-flow experiments performed in the −40 to 0 °C temperature range revealed a very similar second-order decomposition of **1**·O_2 in acetonitrile (Figure S1). However, the solvent had to be doubly distilled to obtain the second-order behavior; otherwise, the kinetic traces were more complex and poorly reproducible, possibly arising from a combination of first- and second-order processes. The unusual second-order nature of the decomposition reaction was confirmed by excellent fits of the experimental kinetic traces to a second-order equation, and by the independence of the second-order rate constant on the initial concentration of the peroxo species. As expected, the initial rates of the peroxide decomposition depended dramatically on the complex concentration. These reaction rates and the activation parameters derived from them were also similar to those reported by Feig et al. (Table 6).[19]

Table 6. Kinetic Parameters for the Decay of Diiron(III)−Peroxo Complexes

complex, solvent	order	$\Delta H^{\ddagger}$, KJ mol^{-1}	$\Delta S^{\ddagger}$, J $K^{-1}mol^{-1}$	ref
1, CH_3CH_2CN	2nd	51.9 ± 2.7	22 ± 6[b]	19
1, CH_3CN	2nd	44 ± 5	-21 ± 16	*a*
1, CH_3CN, 20 equiv Ph_3PO	2nd	40 ± 4	-97 ± 16	*a*
1, CH_2Cl_2/DMSO (9:1 v/v)	1st	49 ± 4	-79 ± 12	*a*
3, CH_2Cl_2/DMSO (9:1 v/v)	1st	60 ± 4	-50 ± 8	*a*
6, CH_2Cl_2	1st	103 ± 4	59 ± 15	*a*
$[Fe_2(N\text{-Et-HPTB})(OBz)]^{2+}$, CH_3CH_2CN	2nd	80.6 ± 3.9	74 ± 14	19
$[Fe_2(N\text{-Et-HPTB})(OBz)]^{2+}$, CH_2Cl_2	1st	66.6 ± 3.3	-40 ± 20	15
MMOH (H_2O)	1st	114	163	48
Δ9D (H_2O)	1st	80	−41	49

[a] This work. [b] $\Delta S^{\ddagger}$ was reported by Feig et al.[19a] as -47 ± 11 J K^{-1} mol^{-1}, but a reexamination of the data provided in the supporting material shows that the activation entropy should be changed to the value listed in this table.[19b]

As previously observed for $[Fe_2(N\text{-Et-HPTB})(O_2)(O_2CR)]^{2+}$, the addition of Ph_3PO to **1**·O_2 greatly stabilized the intermediate and allowed its decay to be monitored by conventional UV−vis spectroscopy. Kinetic analysis revealed that the decay of **1**·O_2 remains a second-order process, whose rate is inversely proportional to Ph_3PO concentration (Figure S2). This observation strongly suggests that added Ph_3PO is

involved in a binding preequilibrium that limits the concentration of the species that undergoes second-order decay.

Stopped-flow studies of the reaction of **1** with O_2 in CH_2Cl_2 indicated that the decay of **1**·O_2 in this solvent was similar to that in CH_3CN and thus not investigated in detail. However, when a 9:1 (v/v) mixture of CH_2Cl_2/DMSO was used as solvent, the **1**·O_2 adduct was significantly stabilized, and the decomposition of **1**·O_2 became a first-order process with a rate constant independent of the concentration of the complex. Considering the importance of using purified solvent in the CH_3CN study, the first-order behavior observed in the presence of DMSO may be due to the introduction of an impurity present in DMSO or due to a change in mechanism. In any case, it is clear that the nature of the solvent can play an important role in determining the mechanism of peroxide decomposition.

The activation parameters for the decay of **1**·O_2 under different conditions as well as that for **3**·O_2 in CH_2Cl_2/DMSO are collected in Table 6, and Eyring plots are collected in Figure S3. While the activation enthalpies for peroxo decay in acetonitrile, propionitrile, and CH_2Cl_2/DMSO fall within a relatively narrow range of 40−60 kJ mol^{-1} K^{-1}, the obtained activation entropies show much greater variability, ranging from +22 to −97 J mol^{-1} K^{-1}. It is difficult to rationalize the observed differences in the light of the distinct molecularities of the decay processes, but the decomposition of these peroxo intermediates is very likely a multistep reaction, thereby complicating the molecular interpretation of the activation parameters.

Relative to the O_2 adducts of the monocarboxylate-bridged complexes, the **6**·O_2 intermediate is even more stable. It decomposes via a first-order process in pure CH_2Cl_2, with a rate constant that is independent of the concentration of complex. At 0 °C, the rate of decomposition is 1.43×10^{-4} s^{-1}, compared to a calculated value of 1.45×10^{-1} s^{-1} for **1**·O_2 in CH_2Cl_2/DMSO (9:1 v/v) obtained by extrapolation of the corresponding Eyring plot. In other words, the introduction of the second carboxylate group enhances the stability of the peroxide by 3 orders of magnitude over that of **1**·O_2, already stabilized by the presence of DMSO. The higher stability of **6**·O_2 is reflected by a 50 kJ mol^{-1} higher activation enthalpy. Opposite to **1**·O_2, the activation entropy for the decay of **6**·O_2 is positive and indicative of a dissociative mechanism. Given the instability of the monocarboxylate peroxo adduct in the absence of DMSO, it is reasonable to propose that the complete dissociation of the second carboxylate may be the rate determining step in the decomposition of **6**·O_2**.** The observed high barrier can easily be rationalized by the charge separation required for complete dissociation. However, the rate of decay of **6**·O_2 was found to be independent of added $ArCO_2^-$. Furthermore, the decay of **1**·O_2 in CH_3CN could be dramatically suppressed in a double mixing stopped-flow experiment by adding either 1 or 20 equiv of benzoate ion after formation of **1**·O_2 but prior to its decay. This result shows that binding of the added benzoate to **1**·O_2 is rapid and a rapid pre-equilibrium between **1**·O_2 and **6**·O_2 is quite unlikely to be a factor in the mechanism of decomposition.

The effects of benzoate ring substituents on the rates of decomposition of a series of O_2 adducts of mono- and dicarboxylate-bridged diiron(II) complexes were also investigated. As shown in Figure 8, the decay rates for the peroxo intermediates from monocarboxylate precursors correlate with Hammett σ values to give a ρ value of −1.1. Hence, increasing the donating ability of the carboxylate diminishes the stability of the peroxide, as previously observed for related O_2 adducts of [Fe_2(*N*-Et-HPTB)(O_2CR)] complexes.[15] In sharp contrast, the decay rates for the dicarboxylate O_2 adducts were not significantly affected by the different substituents on the carboxylates. This strongly suggests that the stability conferred to the peroxide intermediate by the second carboxylate is due not to electronic factors but instead to the coordinative saturation of the metal center.

Substrate Oxidation Studies. The oxidative abilities of the O_2 adducts versus different substrates were investigated. Due to its short lifetime in CH_3CN solvent, the reaction of **1**·O_2 with Ph_3P was monitored with double-mixing stopped-flow methodology. The short-lived **1**·O_2 was generated in the first mixing loop, and the substrate was added in the second mixing step with a fixed time delay that ranged from 500 ms at −40 °C to 40 ms at 0 °C. In all experiments, the rate of decomposition of **1**·O_2 was accelerated 10- to 100-fold upon addition of Ph_3P (Figure 9). The reaction kinetics, however, were complicated and could not be adequately fit to either a pseudo-first-order or a second-order process. The initially rapid reaction slowed with time. Most likely, this behavior could be attributed to product inhibition. The oxidation of Ph_3P yields Ph_3PO that effectively competes with PPh_3 for the labile coordination sites of **1**·O_2 (X and Y in Scheme 2).

The kinetic behavior of **1**·O_2 with PPh_3 was simpler in CH_2Cl_2/DMSO (9:1 v/v). Figure 10 shows that the rate of first-order decay of **1**·O_2 increases linearly with PPh_3 concentration at low concentrations but plateaus at higher concentration. This saturation behavior indicates a preequilibrium binding of PPh_3 to the diiron center prior to its oxidation by **1**·O_2, i.e.

$$[(HPTP)Fe_2(OBz)(O_2)]^{2+} + PPh_3 \underset{k_{-1}}{\overset{k_1}{\rightleftharpoons}} [(HPTP)Fe_2(OBz)(O_2)(PPh_3)]^{2+} \quad (1)$$

$$[(HPTP)Fe_2(OBz)(O_2)(PPh_3)]^{2+} \xrightarrow{k_2} [(HPTP)Fe_2O(OBz)]^{2+} + OPPh_3 \quad (2)$$

By incorporating a pre-equilibrium step, the rate law can be expressed as eq 3:

$$-d[\mathbf{1}\cdot O_2]/dt = k_2K_1[\mathbf{1}\cdot O_2][PPh_3](1 + K_1[PPh_3])^{-1} \quad (3)$$

From the double reciprocal plot shown in Figure 10 inset, the K_1 of this pre-equilibrium is estimated to be 120 M^{-1} at −40 °C. Thus, PPh_3 must bind to the diiron−peroxo intermediate prior to being oxidized.

Studies of the reactivity of **1**·O_2 with other substrates in CH_2Cl_2/DMSO (9:1 v/v) at −40 °C are listed in Table 7.

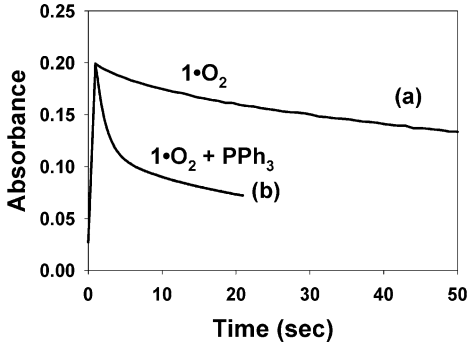

Figure 9. Decomposition of **1**·O_2 generated at −40 °C in a stopped-flow mixing cell: (a) in pure CH_3CN; (b) in the presence of PPh_3 added in the second mixing loop. Initial concentrations of reagents in the mixing cell: [**1**] = 0.250 mM; [O_2] = 2.03 mM; [PPh_3] = 1.00 mM; solvent, CH_3CN.

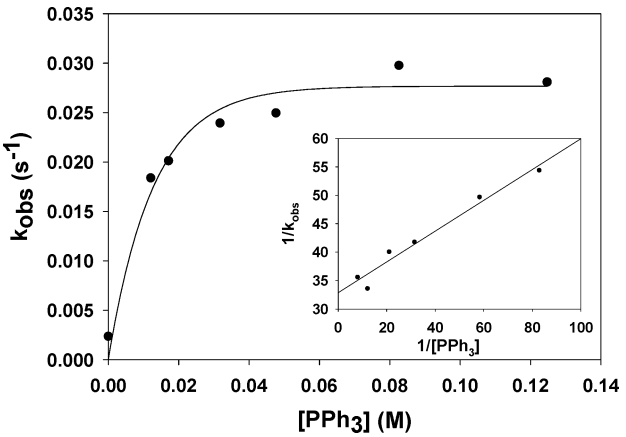

Figure 10. Dependence of the rate of decay of **1**·O_2 in CH_2Cl_2/DMSO (9:1 v/v) at −40 °C with added PPh_3.

Table 7. Oxidation Reactions of **1**·O_2 and **6**·O_2[a]

substrate	product	% yield from [**1**·O_2]	% yield from [**6**·O_2]
PPh_3	$OPPh_3$	100	n.r.[b]
methyl phenyl sulfide	methyl phenyl sulfoxide	59	n.r.[b]
thiophenol	diphenyl disulfide	100	
3,5-di-*tert*-butyl-catechol	3,5-di-*tert*-butyl-quinone	100	
benzyl alcohol	benzaldehyde	100	n.r.[b]
cyclohexanol	cyclohexanone	23	
9,10-dihydroanthracene	anthracene	n.r.[b]	n.r.[b]

[a] The 60 mM substrate reacted with 3 mM **1**·O_2 in CH_2Cl_2/DMSO (9:1 v/v) or **6**·O_2 in CH_2Cl_2 at −40 °C. [b] n.r. = no reaction.

Complex **1**·O_2 effects efficient oxidation of methyl phenyl sulfide to the sulfoxide, without any overoxidation to the sulfone. Similarly to what was observed with the addition of PPh_3, the rate of decay of **1**·O_2 is accelerated by the increase of the concentration of substrate, suggesting that the peroxo complex itself is responsible for the oxygen transfer to the substrate. The peroxo complex also quantitatively oxidizes thiophenol to the corresponding disulfide and 3,5-di-*tert*-butylcatechol to the quinone. With respect to alcohols, benzyl alcohol is oxidized quantitatively to benzaldehyde, but cyclohexanol with the stronger α-C−H bond is oxidized to cyclohexanone only in 23% yield. In contrast, **1**·O_2 does not oxidize 9,10-dihydroanthracene at all, despite that the fact that its C−H bonds are somewhat weaker than those of benzyl alcohol (78 vs 81 kcal/mol).[53] Such a lack of hydrogen atom abstraction ability argues against the participation of high valent species in the decomposition of the peroxo intermediate, which would be expected to be good hydrogen atom abstracting agents and thus effective in oxidizing substrates such as dihydroanthracene. What distinguishes dihydroanthracene from the other substrates listed in Table 7 is its inability to coordinate to the diiron center. We thus propose that the oxidation of the substrates listed in Table 7 involves initial coordination to the peroxo intermediate and subsequent reaction with the metal-bound peroxide. In support of this inner sphere oxidation mechanism, we note that the coordinatively saturated **6**·O_2 is unable to oxidize PPh_3, benzyl alcohol, methyl phenyl sulfide, nor 9,10-dihydroanthracene, presumably because these potential substrates lack sufficient affinity for iron(III) to displace one of the bound carboxylates in **6**·O_2.

Conclusions

In this paper, we have synthesized and characterized a series of diiron(II) complexes of the dinucleating ligand HPTP supported by one or two carboxylate bridges, in order to examine the role these carboxylates play in the reaction of the diiron(II) complex with O_2. The monocarboxylate-bridged complexes have at least one available coordination site, while the dicarboxylate-bridged complexes are coordinatively saturated. Nevertheless, all complexes bind O_2 in a second-order reaction to form (μ-1,2-peroxo)diiron(III) intermediates. However, the addition of the second bridge results in a decrease of the rate of oxygenation by an order of magnitude, presumably due to a required carboxylate shift from bridging to terminal to open up a site for O_2 binding.

The decomposition of peroxo intermediates derived from monocarboxylate precursors is somewhat complex. It exhibits second-order behavior with respect to diiron complex in organonitrile solvents but becomes first-order in CH_2Cl_2/DMSO (9:1 v/v). Electron withdrawing substituents on the benzoate slow the rate of decomposition, in agreement with an observation made previously for a related series of $[Fe_2(O_2)(N\text{-Et-HPTB})(O_2CAr)]^{2+}$ intermediates.[15] Substrate oxidation follows an inner sphere mechanism, requiring prior coordination of the substrate to an open coordination site on the diiron center and subsequent reaction with the metal-bound peroxide.

The unexpected finding of this work is the remarkable stability of the peroxo species generated from the dicarboxylate-bridged precursors **6**−**10**. IR experiments indicate that the carboxylate bridges in the precursor have become terminal ligands in the O_2 adduct. However, unlike their monocarboxylate analogues, the stability of the peroxo intermediates is not significantly affected by substituents on the benzoates. The stability of the (μ-1,2-peroxo)diiron(III) unit in these complexes is thus determined by the acces-

(53) Bordwell, F. G.; Cheng, J.-P.; Ji, G.-Z.; Satish, A. V.; Zhang, X. *J. Am. Chem. Soc.* **1991**, *113*, 9790−9795.
(54) Broadwater, J. A.; Ai, J.; Loehr, T. M.; Sanders-Loehr, J.; Fox, B. G. *Biochemistry* **1998**, *37*, 14664−14671.

Scheme 3

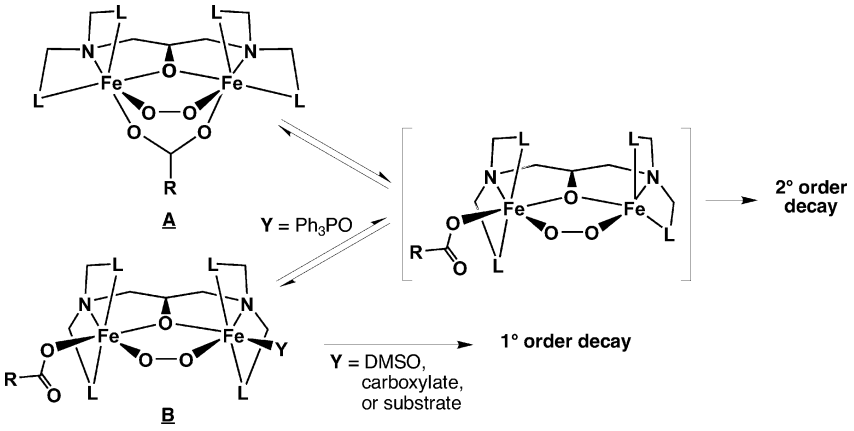

sibility of potential reducing agents to the diiron center. By effectively blocking access, the terminal carboxylates of **6**·O_2 and, by extension, the Ph_3PO ligands of the crystallographically characterized $[Fe_2(O_2)(N\text{-Et-HPTB})(Ph_3PO)_2]^{3+}$ intermediate[15] limit the reactivity of the diiron(III)−peroxo species and enhance the thermal stability of these intermediates.

These observations can be rationalized by the mechanistic picture shown in Scheme 3. The monocarboxylate-bridged diiron(II) precursor reacts with O_2 to form adduct A, which decays rapidly via a second-order process. In the presence of an oxygen donor ligand like Ph_3PO, DMSO, or a second carboxylate, the O_2 adduct becomes stabilized as structure B. Adduct decay can be initiated by dissociation of Y. In polar CH_3CN, the dissociation of Ph_3PO is facile, and the peroxo decomposition retains its second-order character. However, in less polar CH_2Cl_2, ligand dissociation is less facile and can become partially rate determining. Such a situation is suggested by the more complex kinetics of peroxo decay in the presence of 20 equiv of Ph_3PO. When Y is a second carboxylate, dissociation of Y becomes kinetically and thermodynamically unfavorable, and a slow first-order decomposition of a coordinatively saturated peroxo complex B dominates. Furthermore, substrates that can occupy site Y are oxidized, and the **1**·O_2·substrate adduct decays in a first-order process with the peroxide attacking the substrate in the metal coordination sphere.

Extrapolation of these notions to the reactivity of diiron(III)−peroxo species in biology suggests the following insight. The hydrocarbon substrates of methane monooxygenase and fatty acid desaturases are unlikely to be oxidized by their respective (μ-1,2-peroxo)diiron(III) intermediates[48,49,54] by a direct coordination mechanism as found for the synthetic analogues, since such substrates cannot coordinate to the diiron center. Thus, their oxidation may occur by proximity to the diiron centers or may require some activation step, perhaps protonation of the bound peroxide, that promotes cleavage of the O−O bond prior to substrate oxidation. Indeed, such a protonation step is strongly implicated by the pH dependence observed for the conversion of peroxo intermediate **P** to high valent intermediate **Q** in single turnover studies of methane monooxygenase.[55]

Acknowledgment. This work was supported by NIH Grant GM-38767 to L.Q. and NSF Grant CHE0111202 and Research Corporation Grant RI0223 to E.V.R.-A. M.C. thanks Fundacio La Caixa for a postdoctoral fellowship that supported in part his stay at the University of Minnesota. M.J.R. was supported by the Lando Summer Research Fellowship Program, while C.W.C. was supported in part by a grant from the University of Minnesota's Undergraduate Research Opportunities Program.

Supporting Information Available: X-ray crystallographic file for $[Fe^{II}_2(HPTP)(O_2CC_6F_5)(CH_3CN)](BPh_4)_2\cdot CH_3CN$ (**3**) and $[Fe^{II}_2(HPTP)(O_2CC_6H_5)_2](BF_4)\cdot CH_3CN$ (**6**) in CIF format and a pdf file containing Tables S1 and S2, respectively, listing NMR shifts of diiron(II) complexes **1**−**10** and the absorption maxima of corresponding O_2 adducts, Figure S1 showing kinetic data for the decomposition of **1**·O_2 in CH_3CN, Figure S2 showing the effect of added $OPPh_3$ on the decay of the O_2 adduct of **1**, and Figure S3 showing Eyring plots for the decomposition of the diiron(III)−peroxo intermediates. This material is available free of charge via the Internet at http://pubs.acs.org.

IC034359A

(55) Lee, S.-K.; Lipscomb, J. D. *Biochemistry* **1999**, *38*, 4423−4432.